Hindawi
Journal of Engineering
Volume 2019, Article ID 6413608, 10 pages
https://doi.org/10.1155/2019/6413608

Research Article

Wear Inducing Phase Transformation of Plasma Transfer Arc Coated Tools during Friction Stir Welding with Al Alloy

Kuan-Jen Chen,[1] **Fei-Yi Hung**,[2] **Truan-Sheng Lui**,[2] **and Yong-Ren Shih**[2]

[1] *The Instrument Center, National Cheng Kung University, Tainan 701, Taiwan*
[2] *Department of Materials Science and Engineering, National Cheng Kung University, Tainan 701, Taiwan*

Correspondence should be addressed to Fei-Yi Hung; fyhung@mail.ncku.edu.tw

Received 9 August 2018; Accepted 26 November 2018; Published 1 January 2019

Guest Editor: Long Wan

The friction stir welding process (friction stir welding/processing, FSW/FSP) has wear problems related to stirring tools. In this study, the plasma transfer arc (PTA) method was used with stellite 1 powders (Co-based) to coat on the head of a SKD61 stirring tool (SKD61-ST1) in order to investigate the wear performance and phase transformation of SKD61-ST1 after FSW. Under the same experimental parameters, the wear data were compared with the high-speed steel SKH51 (tempering material SKH51-T and annealed material SKH51-A) and tungsten-carbide cobalt (TCC). Results showed the PTA coating was a γ-Co solidification matrix with M_7C_3 and $M_{23}C_6$ carbides. After FSW, the wear resistance of SKD61-ST1 was better than that of SKH51-A and SKH51-T and lower than that of TCC. The SKD61-ST1, SKH51-A, and SKH51-T stirring tools exhibited sliding wear after FSP, where the pin and shoulder of the stirring tool formed a phase transfer layer on the surface, and the peeling of the phase transfer layer caused wear weight loss. The main phase of the phase transfer layer of the SKD61-ST1 tool was Al_9Co_2. The affinity and adhesion energy of the Co-Al phase was lower than that of Fe-Al phase, and the phase transfer layer of the SKD61-ST1 tool was thinner and had lower coverage, thereby increasing the wear resistance of the SKD61-ST1 stirring tools during FSW.

1. Introduction

Temperature of friction stir welding (FSW) occurs under the melting point of metal and thus can prevent typical solidification defects of traditional joining methods [1]. FSW can induce frictional heat and plastic metal flow, generating dynamic recrystallization, grain refinement, and second phase refinement that enhances the mechanical properties of materials [2, 3].

In recent years, FSW has been widely used in Al alloys, but the stirring rods have wear problems and reduce the life of the stirring rods [4–6]. Tungsten carbide (WC) is extremely hard; therefore tools are often made with WC and cobalt alloy powders to form high wear-resistance tungsten-carbide cobalt (TCC) materials using a sintering process. The use of a TCC stirring rod can increase wear performance and life, but it is expensive. Therefore, developing a new stirring tool that meets the need for appropriate wear conditions and affordability is necessary. SKH51 is one of the most commonly used high-speed tool steels. Under high-speed conditions, it can still maintain good mechanical properties, and its price is lower than that of TCC, so it is often used as a stirring tool in FSW [7].

The SKD61 is a tool steel with good thermal-crack resistance, and it is cheaper than SKH51 [8]. Coating on the pin of an SKD61 stirring rod for FSW causes a better wear resistance. The plasma transferred arc (PTA) process is a surface coating treatment [9, 10]. The plasma arc between the electrode and the substrate is used to coat the alloy powders on the substrate to form a highly wear resistant coating layer. PTA has many characteristics: (1) The PTA-overlay is thicker than a laser induced overlay. Because the PTA-overlay is metallurgical bond, its impact-resistance is higher. (2) The powder can be selected at random, and the composition of the overlayer can be established easily. (3) The working distance between the electrode and work-surface is more flexible. The PTA process has higher work efficiency and is commonly used in surface-overlaid manufacturing.

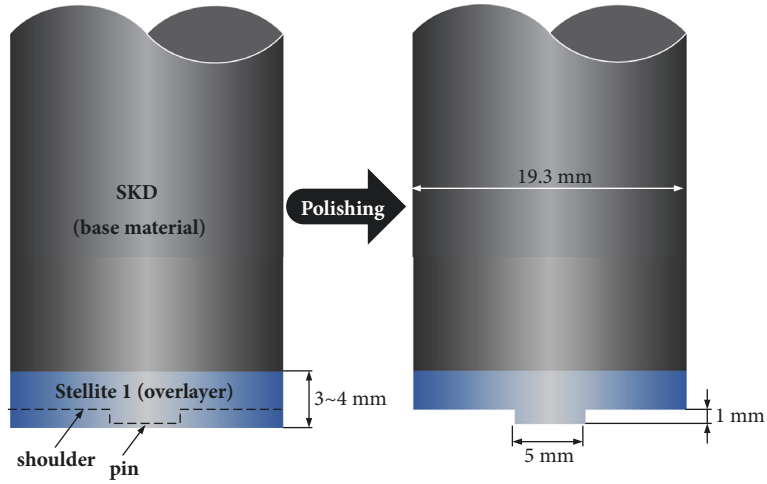

Figure 1: Stellite overlayer processing to the pin and shoulder.

In addition, stellite 1 powders had good wear resistance and thermal shock properties and therefore are often used as a coating material [11].

For above reasons, this study used PTA process to coat stellite 1 powders on SKD61 alloy steel to form the stirring tool (SKD61-ST1). The coating structure of the SKD61-ST1 tool was investigated and also used in FSW for a 5083 aluminum alloy substrate to discuss the wear characteristics. Notably, the stirring wear rates of SKH51 high-speed steels (annealed SKH51-A and tempering SKH51-T) and TCC were compared with SKD61-ST1 under the same experimental parameters. In addition, the wear mechanism (wear induced phase transformation) of SKD61-ST1 was investigated. The phase transformation of the stirring tool can confirm the wear fracture characteristics, and the correlation data may serve as a reference for the application of a FSW system.

2. Experimental Procedure

2.1. Stirring Tool Preparation. PTA coated stellite 1 powders were used on the surface of SKD61 mold steel to form an SKD61-ST1 stirring rod. SKH51 high-speed steel (SKH51-A) was annealed, underwent oil quenching, and was then tempered to form an SKH51 high-speed steel tempering material (SKH51-T: oil quenching at 1230°C for 4 minutes; tempering at 560°C for 2 hours). This experiment involved the use of four stirring rods: (1) SKD61-ST1, (2) SKH51-A, (3) SKH51-T, and (4) TCC. FSW performed four rods in a 5083 aluminum alloy substrate in order to acquire the wear data for the stirring rods under the same experimental parameters. After the FSW, the pin edge of the stirring rod was observed, and the hardness of the head of the stirring rod was measured. Scanning electron microscopy (SEM), energy dispersive spectroscopy (EDS), electron probe X-ray microanalyzer (EPMA), and X-ray diffraction (thin film XRD) were used to investigate the wear characteristics and wear induced phase transformation.

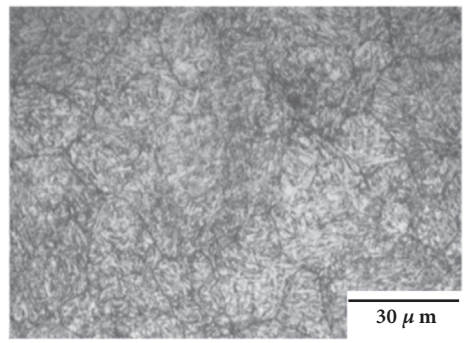

Figure 2: OM metallurgical phase of the SKD61 annealing material.

2.2. Coating of the SKD61 Tool Using the PTA Process. Stellite 1 powders were coated on the head of the SKD61 stirring rod, the thickness of the stellite 1 overlayer was 3~4 mm. To polish the stellite 1 overlayer, a pin with a height of 1 mm and a diameter of 5 mm was formed on the surface of the shoulder with a diameter of 19.3 mm. A schematic diagram of the SKD61-ST1 stirring rod is shown in Figure 1. Notably, the pin, shoulder, and friction stir zone were SKD61-ST1 (stellite 1 overlayer structure). In addition, SKD61 matrix was an annealed structure and the hardness was about 24 HRC. The microstructure and chemical composition are shown in Figure 2 and Table 1. The chemical composition of stellite 1 powders is provided in Table 2, and the PTA experimental parameters are shown in Table 3.

2.3. Wear Measurement and Subsurface Observation of the Stirring Rod. The SKD61-ST1, SKH51-A, SKH51-T, and TCC stirring rods were the same size (Figure 1) and underwent the friction stir test under the same experimental parameters. The stirred substrate was the annealed 5083 aluminum alloy, and the walking distance for every stirring rod was five meters (each walk was 0.5m, which was then stopped and cooled for

Table 1: Chemical composition of the SKD61 mold steel (PTA coated substrate) (wt.%).

C	Si	Mn	P	S	Cr	Mo	V	Fe
0.35	0.80	0.40	0.02	0.02	4.50	1.20	1.00	Bal.

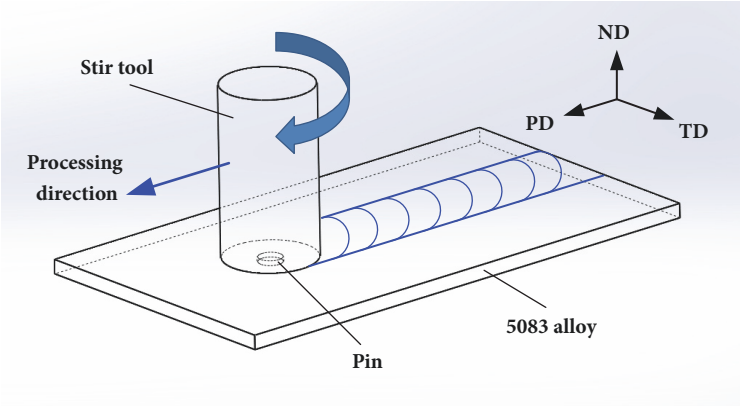

Figure 3: Schematic diagram of the friction stir process.

Table 2: Chemical composition of the stellite 1 cobalt-based alloy (PTA coating powder) (wt%).

Cr	C	W	Si	Co
32.00	2.50	11.50	2.00	Bal.

Table 3: PTA process parameters.

Powder flux	1200 g/hr
Plasma gas (Ar)	4 l/min
Powder delivery gas (Ar)	3 l/min
Shielding gas (Ar)	24 l/min
Overlay current	90A
Overlay voltage	36V

Table 4: The friction stir process (FSP) parameters.

Stirring rod speed	1256 RPM
Specimen feed rate	4 mm/s
Stirring rod tilt angle	1.5°
Under pressure	43.4 MPa
Stirred material	Annealed 5083 Al alloy
Stirred substrate size	$150 \times 46 \times 13$ mm^3
Walking distance	5 m

five minutes, and repeated 10 times). The speed and feed rate of the stirring rod were 1256 rpm and 4 mm/s, respectively. The parameters for the FSW test are shown in Table 4. Figure 3 is a schematic diagram of the FSW. The microstructure and chemical composition of the 5083 aluminum alloy are shown in Figure 4 and Table 5.

Before and after the FSW, the weight of stirring rod was measured to obtain the wear rate. After the FSW, the head of the stirring was adhered to the 5083 aluminum alloy, so the stirring head was put into an aqueous solution of 50 wt.% NaOH to remove the 5083 aluminum alloy and then the weight loss was measured.

2.4. Observation of Wear Subsurface. After the FSW, the pin and shoulder of the SKH51-A, SKH51-T, and SKD61-ST1 stirring rods were cut to observe the worn subsurface using SEM, EDS, and EPMA. In addition, the coverage area, hardness, and thickness of wear inducing a new phase on the pin and shoulder of the stirring rods were measured, for which the measurement data was the average of 10 values. The wear inducing phases by FSW on the pin surface were identified using thin film XRD. Notably, the wear inducing phases was removed and then detected the structure of the pin to confirm the wear phase transformation.

3. Results and Discussion

3.1. Solidification Structure of PTA Coated Stellite 1 on SKD61 Steel. Using a PTA coated stellite 1 cobalt-based superalloy on SKD61 steel, the cross-section of the coated specimen was observed, as shown in Figure 5. The coating specimens can be divided into three parts, (1) stellite 1 overlayer, (2) the interface region, and (3) the SKD61 base material.

From the literature [12, 13], the different overlaying currents will affect the degree of dilution effect between the substrate and the overlayer. In this study, the interface region is set to zero; the overlayer is in a forward direction, and the semiquantitative composition and microhardness of the subsurface of the coated specimens were analyzed. Figure 6 shows that the iron content of the overlayer decreased less than 3 wt.% at the 0.8 mm site using a 90A coated current. In addition, the microhardness values did not significantly change when the detected zone was not in the interface region (Figure 7). This can explain why the dilution effect between SKD61 base material and the stellite 1 overlayer was not obvious.

Table 5: Chemical composition of 5083 aluminum alloy (wt.%).

Si	Fe	Cu	Mn	Mg	Sn	Ti	Cr	Al
0.40	0.40	0.10	0.45	4.50	0.25	0.15	0.05	Bal.

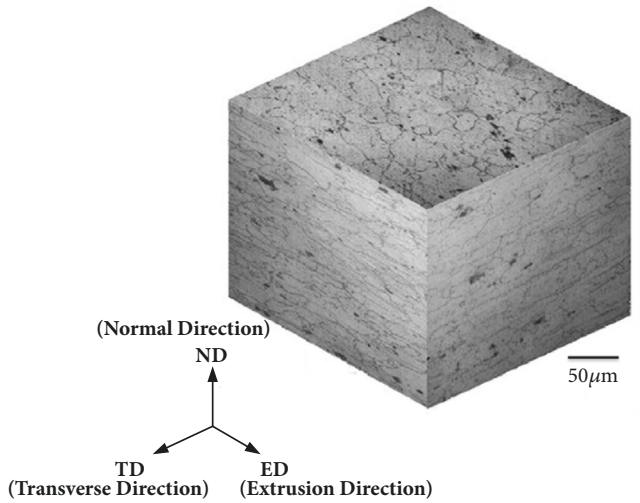

Figure 4: Microstructure of 5083 aluminum alloy annealed materials.

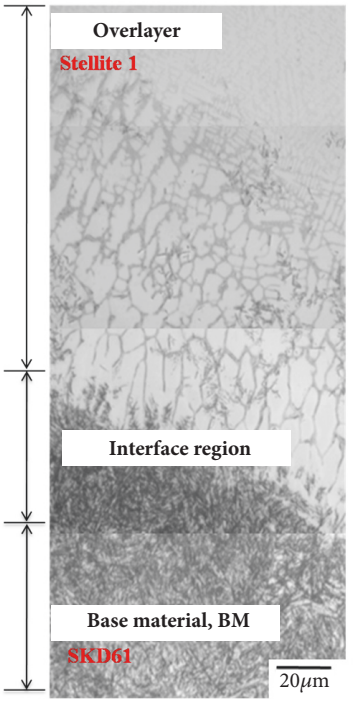

Figure 5: The PTA coated stellite 1 SKD61 substrate: OM metallographic transverse cross-section coated specimen.

The stirring rod matrix was an annealed SKD61 steel, for which the matrix was ferrite, and M_6C carbides were dispersed in the matrix [14]. Figure 8 shows the solidification structure in the stellite 1 overlayer (the pin and shoulder of the stirring rod), for which the hardness was 56 HRC. X-ray diffraction showed the overlay to be a γ-Co matrix with an FCC structure containing M_7C_3 and $M_{23}C_6$ carbides (Figure 9). In previous studies [12], M_7C_3 and $M_{23}C_6$ carbides appeared to be massive and fishbone-like, as shown in Figure 10. The interface region is a mixing area formed by SKD61 and stellite 1.

3.2. Wear Rate of the SKD61-ST1, SKH51-A, SKH51-T, and TCC. SKD61-ST1, SKH51-A, SKH51-T, and TCC stirring rods

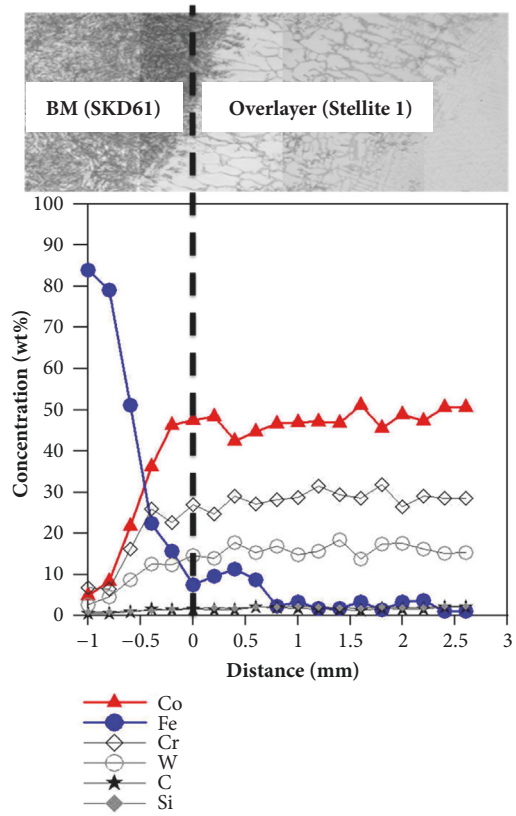

Figure 6: The PTA coated stellite 1 SKD61 in the SEM/EDS analyses.

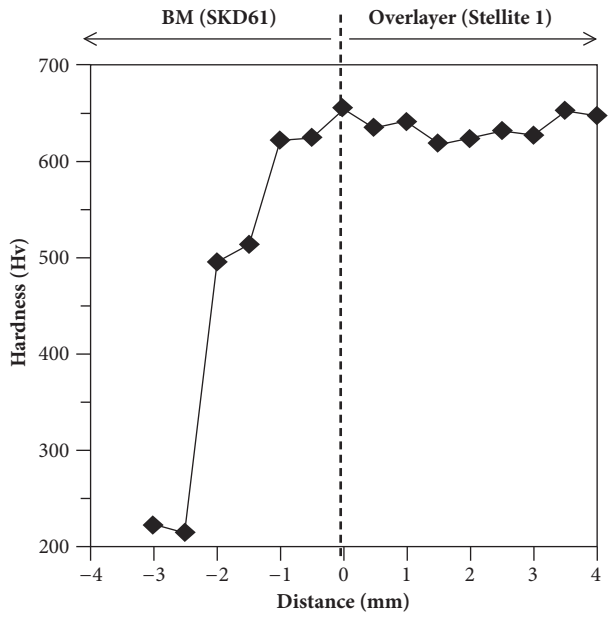

Figure 7: PTA coating stellite 1 measured in the SKD61 for microhardness.

walked 5 meters under the same FSW process conditions after removal of the 5083 aluminum alloy adhering to the stirring rods in order to measure the wear rate of the four stirring rods. Figure 11 shows that the SKH51-A stirring rod had the maximum wear rate and that the SKH51-T stirring rod could significantly enhance the wear resistance. It should be noted that the wear rate of the SKD61-ST1 stirring rod was lower than that of the SKH51-T stirring rod, and its wear rate was closest to that of the TCC stirring rod. Obviously, the cost of the new SKD61-ST1 stirring rod was not only less than that of SKH51 high-speed steel but also had better wear performance in the FSW.

3.3. Wear Mechanism of the SKD61-ST1 Stirring Rod. After the FSW, a cross-section of the stirring rod was taken at the head prior to removal of the SKD61-ST1 aluminum alloy to observe and compare the hardness of the stirring heads before and after the FSW. The original hardness of the stirring head was 56 HRC, and after FSW, it was 54 HRC, so there was no significant difference. The observations of the high temperature wear on the stirring rod shoulder and pin are shown in Figure 12 (the characteristics of the pin edge after FSW).

Symbol E shows the left of interface between the induced new microstructure and stellite 1. Symbol D shows the new microstructure on the pin of the stirring rod after FSW associated with the interaction with the 5083 aluminum alloy, which contained dark (Dd) + white (Dw) mixed structures. C shows the 5083 aluminum alloy adhering on the surface of the stirring pin. The semiquantitative data on the surface

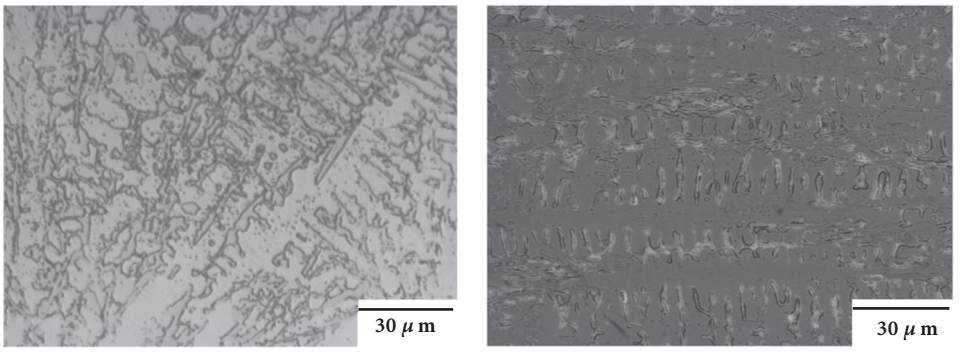

Figure 8: The solidification structure of the stellite 1 overlayer: (a) OM images; (b) SEM images.

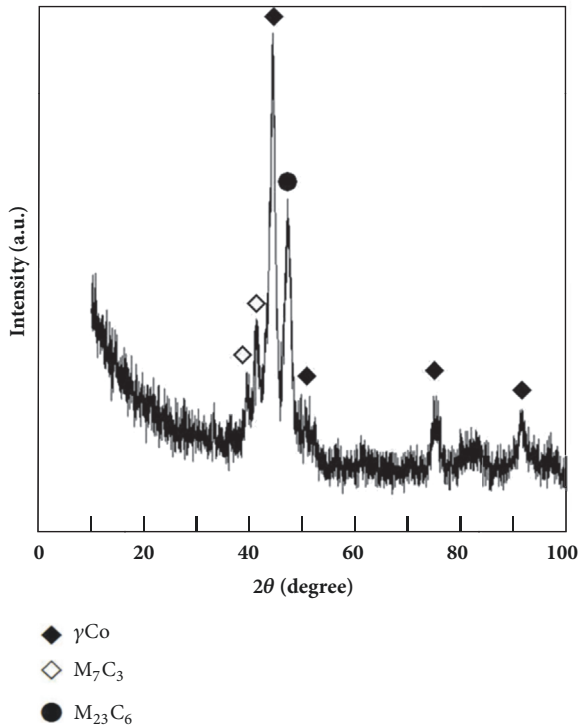

Figure 9: X-ray diffraction pattern of the stellite 1 overlayer.

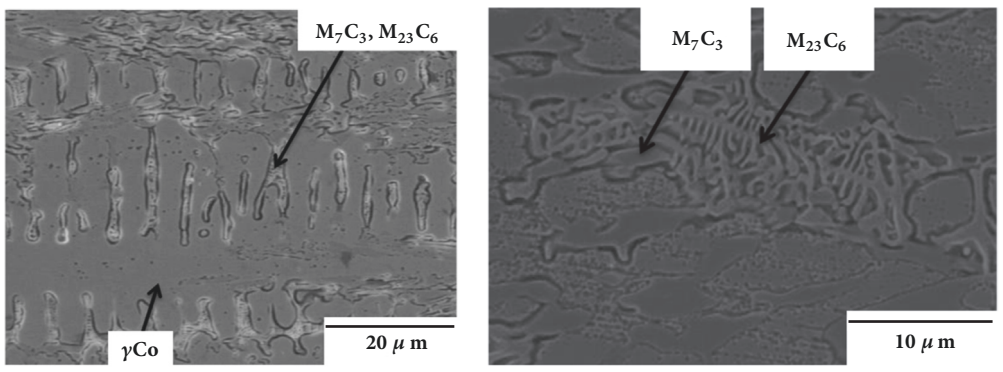

Figure 10: 90A current of the stellite 1 alloy on the SKD61 tool steel, carbide overlayer: (a) low-magnification; (b) high-magnification SEM microscopic observations.

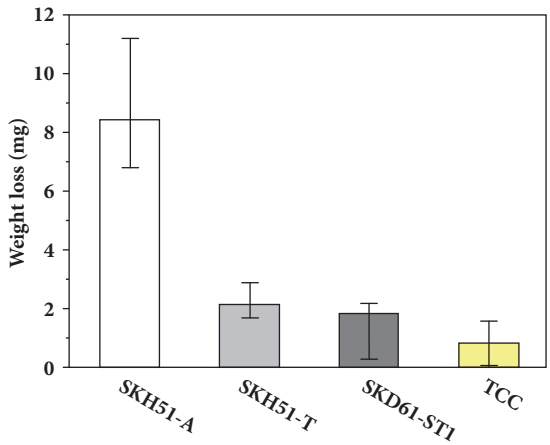

Figure 11: The wear resistance of the SKD61-ST1, annealed SKH51 (SKH51-A), tempered SKH51 (SKH51-T), and tungsten-carbide cobalt (TCC) stirring tool after FSW walking five meters and measurement of the amount of wear.

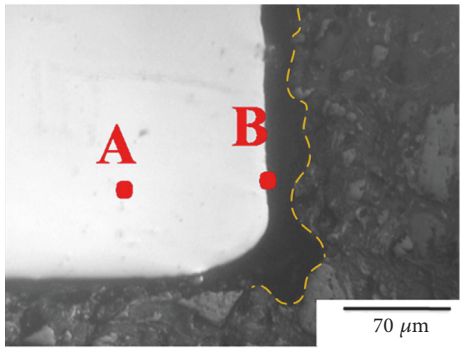

Figure 12: SKD61-ST1 stirring tool after FSW running five meters; observation of the pin edge.

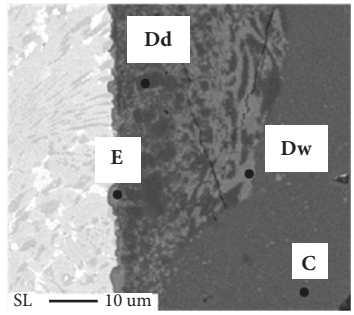

Position / Elements	C	Dd	Dw	E
Mg	6.02	29.05	26.86	5.76
Al	91.16	24.60	32.04	82.10
Mn	2.07	0.61	1.80	--
Si	0.75	4.43	1.21	1.07
O	--	40.24	37.11	2.49
Co	--	--	--	7.84
Cr	--	--	--	0.73

Figure 13: SKD61-ST1 after FSW, SEM-EDS semiquantitative elemental analysis of the pin surface (data for the average of five measurements).

of the stirring rod using EDX are shown in Figure 13. Most of what was left was the stellite 1 cobalt-based superalloy. A nonuniform film was found between the stirring rod and the new structure (E site), for which the composition comprised Co, Cr from the rod-head, and Al, Mg, and Si from the aluminum alloy. The Dd and Dw of new structure contained mainly Al, Mg, and O. The Mg content in the Dd zone was higher than that in Al zone, but the Al content in the Dw zone was higher than that of Mg. The far right C shows the 5083 aluminum alloy.

EPMA mapping was used to detect the element distribution of Figure 13, as shown in Figure 14. The surface of the stirring pin could be divided into three areas (Figure 14): Part I was the coated structure of the stellite 1 in the stirring head. Part II mainly contained Co and Al. This area incurred sliding wear induced by the phase transformation between aluminum alloy and stellite 1. This area was defined as the phase transfer layer. Its thickness was uneven (average thickness of 0.83 μm). Part III was the secondary transfer layer. The right side of Part III shows the residual 5083 aluminum alloy in the rod-head. According to Figures 12 and 14, Part III was the black-white mixed region. In the FSW process, the aluminum alloy adhering on the rod-head had sustained frictional heat and outside oxygen, which generated the uneven structure with O, Mg, and Al elements.

To understand the phase transfer layer in Part II, in this experiment, NaOH solution was used to remove the residual aluminum alloy on the rod-head (Part III) to expose and obtain the phase transfer layer in Part II (SKD61-ST1-FSP). No. 2000 sandpaper was used to grind the SKD61-ST1-FSW specimen to remove the transfer layer of Part II and obtained the rod-head (Part I). This specimen was called SKD61-ST1-FSW-MOVE. The original specimen without the FSW process was called SKD61-ST1. These three specimens were detected using thin film XRD, for which the results are shown in Figure 15. The signals of the thin film XRD were from the surface of the specimen to 0.3μm within the specimen, where the average thickness of the transfer layer of the SKD61-ST1-FSW specimen was 0.83μm. Therefore, part of the signal was from the transfer layer of Part II. However, the thickness of this layer was uneven, and most of the signals were from Part I of the stirring rod-head base metal. From the diffraction patterns of SKD61-ST1 and SKD61-ST1-FSW, the transfer layer of the 5083 Al alloy and stellite 1 had an Al_9Co_2 phase. Notably, the diffraction peaks of SKD61-ST1 and SKD61-ST1-FSW-MOVE were the same, indicating that the rod-head of the stellite had no phase change either before or after FSW processing.

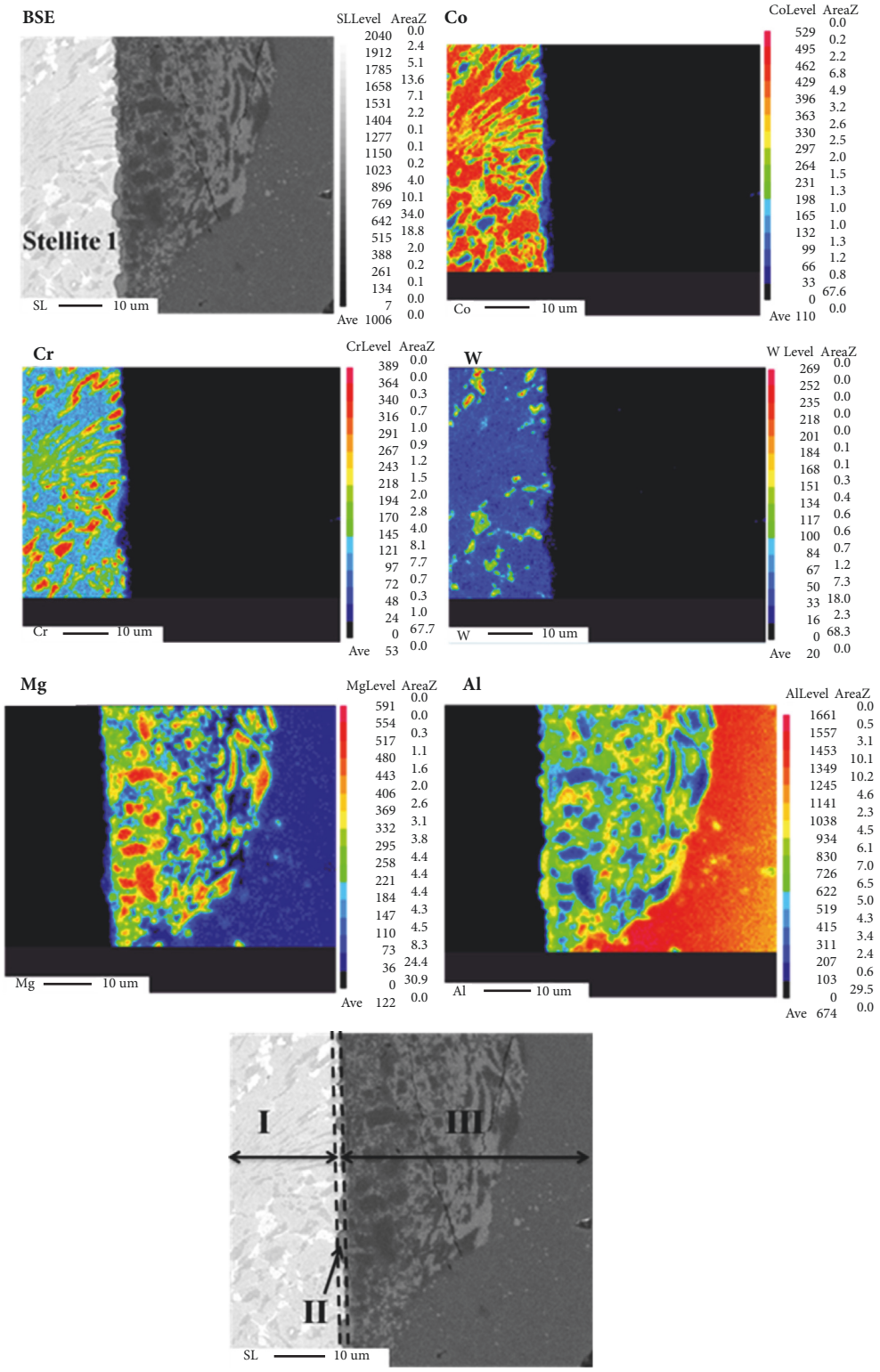

I: Stellite 1
II: transfer layer (0.83 μm)
III: secondary transfer layer

Figure 14: SKD61-ST1 after FSW, EPMA mapping analysis of the pin surface.

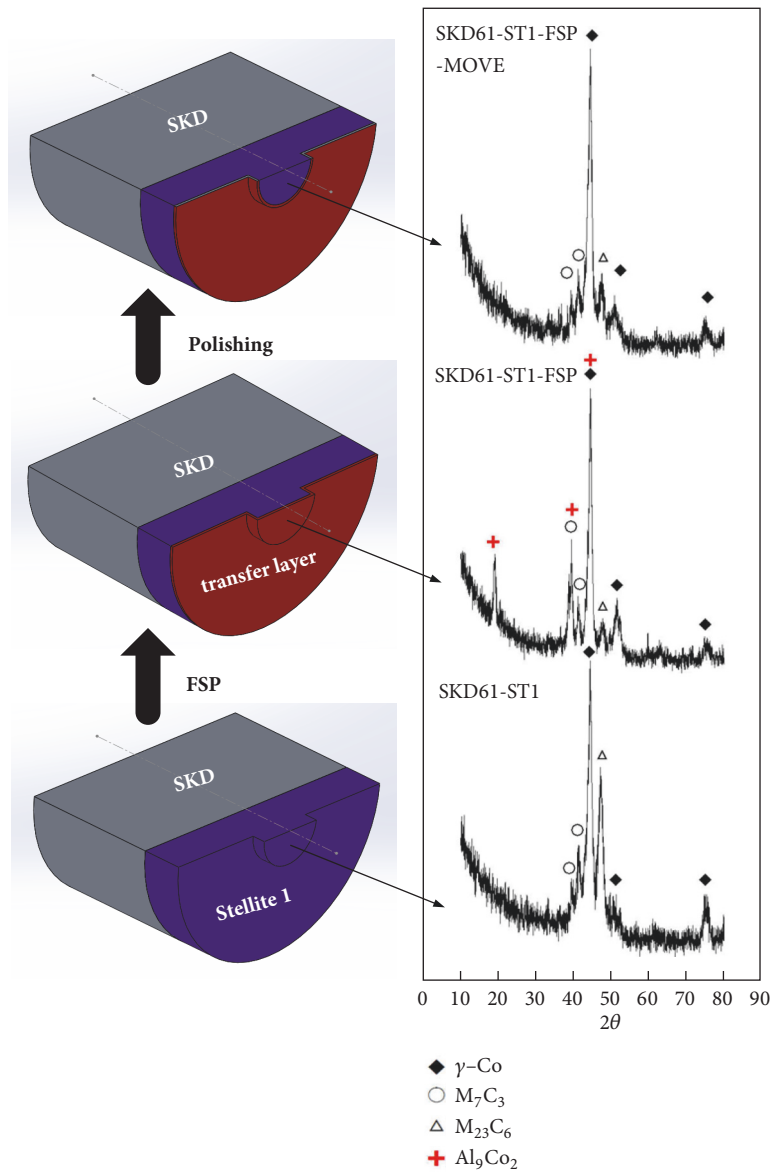

Figure 15: Thin film XRD before and after FSW of SKD61-ST1 spares the rod.

4. Conclusions

(1) Overlayer of stellite 1 was a solid structure containing M_7C_3 and $M_{23}C_6$ carbides. The dilution effect between the SKD61 and the stellite 1 overlayer was not obvious. The overlayer solidification was a γ-Co matrix.

(2) The stellite 1 stirring rod (SKD61-ST1) had better wear resistance, and its wear rate was lower than that of the SKH51 high-speed steel stirring rod. The wear rate of the SKH51-T stirring rod was much lower than that of the SKH51-A stirring rod.

(3) During the FSW, the stellite 1 stirring rod incurred sliding with the 5083 aluminum alloy, and the high temperature created a wear induced phase transfer layer on the pin and shoulder surface of the stirring rods. This transfer layer (Al_9Co_2) peeled and caused mass loss of the stirring rod.

Data Availability

The OM image, SEM/EDS analysis, microhardness, XRD, and EPMA mapping analysis datas used to support the findings of this study are included within the article.

Disclosure

The funders had no role in the design of the study; in the collection, analyses, or interpretation of data; in the writing of the manuscript; and in the decision to publish the results.

Conflicts of Interest

The authors declare no conflicts of interest.

Acknowledgments

The authors are grateful to MOST Instrument Center of National Cheng Kung University (NCKU) and MOST 106-2811-E-006-033 for financial support for this research. This research was funded by the Ministry of Science and Technology (MOST).

References

[1] S. Y. Tarasov, V. E. Rubtsov, and E. A. Kolubaev, "A proposed diffusion-controlled wear mechanism of alloy steel friction stir welding (FSW) tools used on an aluminum alloy," *Wear*, vol. 318, no. 1-2, pp. 130–134, 2014.

[2] S. Chainarong, P. Muangjunburee, and S. Suthummanon, "Friction stir processing of SSM356 aluminium alloy," in *Proceedings of the 12th Global Congress on Manufacturing and Management, GCMM 2014*, pp. 732–740, India, December 2014.

[3] I. G. Papantoniou, H. P. Kyriakopoulou, D. I. Pantelis, A. Athanasiou-Ioannou, and D. E. Manolakos, "Manufacturing process of AA5083/nano-γAl_2O_3 localized composite metal foam fabricated by friction stir processing route (FSP) and microstructural characterization," *Journal of Materials Science*, vol. 53, no. 5, pp. 3817–3835, 2018.

[4] M. Fukumoto, M. Tsubaki, T. Yasui, and Y. Shimoda, "Joining of ADC12 and SS400 by means of friction stir welding," *Welding International*, vol. 19, no. 5, pp. 364–369, 2005.

[5] M. Shamsujjoha, B. K. Jasthi, M. West, and C. Widener, "Friction Stir Lap Welding of Aluminum to Steel Using Refractory Metal Pin Tools," *Journal of Engineering Materials and Technology*, vol. 137, no. 2, p. 021009, 2015.

[6] Y. Wei, J. Li, J. Xiong, F. Huang, F. Zhang, and S. H. Raza, "Joining aluminum to titanium alloy by friction stir lap welding with cutting pin," *Materials Characterization*, vol. 71, pp. 1–5, 2012.

[7] R. T. Lee, C. T. Liu, and Y. C. Chiou, "Experimental investigations on the feeding force and its formation mechanism during friction stir welding of aluminum alloy using a novel dynamometer," *Journal of the Chinese Society of Mechanical Engineers*, vol. 33, pp. 11–19, 2012.

[8] R. Rai, A. De, H. K. D. H. Bhadeshia, and T. DebRoy, "Review: Friction stir welding tools," *Science and Technology of Welding and Joining*, vol. 16, no. 4, pp. 325–342, 2011.

[9] A. Gatto, E. Bassoli, and M. Fornari, "Plasma transferred arc deposition of powdered high performances alloys: process parameters optimization as a function of alloy and geometrical configuration," *Surface and Coatings Technology*, vol. 187, no. 2-3, pp. 265–271, 2014.

[10] A. Degterev, S. Gnyusov, and S. Tarasov, "Structural modification in a re-heated bead-overlapping zone of the multiple-pass plasma-transferred arc Fe-Cr-V-Mo-C coating," *Surface and Coatings Technology*, vol. 329, pp. 272–280, 2017.

[11] M. S. Sawant and N. K. Jain, "Investigations on wear characteristics of Stellite coating by micro-plasma transferred arc powder deposition process," *Wear*, vol. 378-379, pp. 155–164, 2017.

[12] W. S. Chan, T. S. Lui, and L. H. Chen, "Solidification structures in overlaying of cobalt-based superalloy on ferritic spheroidal graphite cast irons by plasma transferred arc process," *Materials Transactions*, vol. 37, no. 1, pp. 50–55, 1996.

[13] H.-M. Lin and T.-S. Lui, "Microstructural characteristics of electric discharge alloyed layers on spheroidal graphite cast iron with different electrode materials," *Materials Transactions*, vol. 53, no. 6, pp. 1184–1190, 2012.

[14] L.-H. Chiu, C.-H. Wu, and H. Chang, "Wear behavior of nitrocarburized JIS SKD61 tool steel," *Wear*, vol. 253, no. 7-8, pp. 778–786, 2002.